

Interconnections between equilibrium topology and dynamical quantum phase transitions in a linearly ramped Haldane model

Utso Bhattacharya and Amit Dutta

Department of Physics, Indian Institute of Technology, 208016, Kanpur

We study the behavior of Fisher Zeros (FZs) and dynamical quantum phase transitions (DQPTs) for a linearly ramped Haldane model occurring in the subsequent temporal evolution of the same and probe the intimate connection with the equilibrium topology of the model. Here, we investigate the temporal evolution of the final state of the Haldane Hamiltonian (evolving with time-independent final Hamiltonian) reached following a linear ramping of the staggered (Semenoff) mass term from an initial to a final value, first selecting a specific protocol, so chosen that the system is ramped from one non-topological phase to the other through a topological phase. We establish the existence of three possible behaviour of areas of FZs corresponding to a given sector: (i) no-DQPT, (ii) one-DQPT (intermediate) and (iii) two-DQPTs (re-entrant), depending on the inverse quenching rate τ . Our study also reveals that the appearance of the areas of FZs is an artefact of the non-zero (quasi-momentum dependent) Haldane mass (M_H), whose absence leads to an emergent one-dimensional behaviour indicated by the shrinking of the areas FZs to lines and the non-analyticity in the dynamical "free energy" itself. Moreover, the characteristic rates of crossover between the three behaviour of FZs are determined by the time-reversal invariant quasi-momentum points of the Brillouin zone where M_H vanishes. Thus, we observe that through the presence or absence of M_H , there exists an intimate relation to the topological properties of the equilibrium model even when the ramp drives the system far away from equilibrium.

I. INTRODUCTION

The investigation of non-equilibrium many body quantum systems has always been a challenging task, both experimentally and theoretically. The recent experimental advances in realisation of closed condensed matter systems via cold atoms [1, 2] in optical lattices have paved the way for addressing unresolved fundamental problems in out of equilibrium strongly correlated systems. Henceforth, experimental studies have been performed to probe intriguing dynamical phenomena like the real time evolution of closed quantum systems in cold atomic gases, [3], prethermalization [4–6], light-cone like propagation of quantum correlations [7], light-induced non-equilibrium superconductivity and topological systems [8, 9] and many-body localization in disordered interacting systems [10]. In parallel, there have been a plethora of theoretical works on e.g., the growth of entanglement entropy following a quench [11], thermalization [12], light-induced topological matters [13–15], dynamics of topologically ordered systems [16–18], periodically driven closed quantum systems [19–23] and many body localization [24, 25], to name a few. (For review, we refer to [26–31].)

One of the emerging features associated with a non-equilibrium quantum many body system is the possibility of dynamical quantum phase transitions in quenched closed quantum systems, introduced by Heyl *et al* [32]: here, non-analytic behavior occurs at critical times in the subsequent real time evolution (following the quench) generated by the time independent final Hamiltonian. To probe DQPTs in a closed quantum system, one prepares a desired final state $|\psi_f\rangle$ of the system by quenching (changing slowly or rapidly) the parameters of the Hamiltonian usually from one phase to another across a

quantum critical point (QCP) [33]. Then, this state is allowed to freely evolve in time with the time-independent final Hamiltonian (H_f) up to a time t (measured from the instant when $|\psi_f\rangle$ is prepared), before taking its overlap with the final state at the start of the free evolution. This so called Loschmidt overlap amplitude (LOA) is denoted by, $G(t) = \langle \psi_f | e^{-iH_f t} | \psi_f \rangle$, where the final state is not an eigenstate H_f . (It should be noted that throughout this paper the Planck constant \hbar is set equal to unity.) Generalization to the complex time (z) plane yields $G(z) = \langle \psi_f | e^{-H_f z} | \psi_f \rangle$ where $z = \text{Re}[z] + it$. Drawing a formal analogy between the inverse temperature (β) and complex time (z) [34–36], we notice that there exists a close similarity between the canonical partition function of an equilibrium classical system $Z(\beta) = \text{tr}(\exp(-\beta H))$ and $G(z)$ which can now be referred to as a dynamical partition function. By extending this analogy with equilibrium classical phase transitions further, one can now define a quantity in the thermodynamic limit for a d -dimensional system with linear dimension L , called the dynamical free energy density

$$f(z) = - \lim_{L \rightarrow \infty} \frac{1}{L^d} \ln G(z).$$

One can then similarly look for zeros of $G(z)$ (equivalently, non-analyticities in $f(z)$) to find the so-called "Fisher zeros" (FZs) residing in the complex z plane. These zeros of the dynamical partition function ($G(z)$) cover lines or areas (more specifically closely spaced points for a finite size systems which form continuous lines or dense areas in the thermodynamic limit) in the complex time (z) plane (depending upon the *effective* dimensionality of the system under consideration). Consequently, when the lines (or areas) of FZs cross the imaginary (real time) axis at dynamical critical (real) times

$t_c = \text{Im}[z_c]$, one observes DQPTs manifested in non-analyticities in $\text{Re}[f(t)]$ (or its time derivative $\text{Re}[f'(t)]$). Evidently, the LOA, i.e., $G(z)$ can only decay to zero, when the prepared many-body final state $|\psi_f\rangle$ becomes orthogonal to its time evolved counterpart after free evolution with H_f .

The occurrence of DQPTs at specific instants of time following a rapid quench of a transverse Ising chain [37] across its QCP was established in Ref. [32] and the lines of FZs were indeed found to cross the real time axis at those instants. This observation has been independently confirmed through several works on quenched one-dimensional (1D) integrable and non-integrable systems [38–53]. Subsequent studies, however, have established that sudden quenching within the same phase of a system (both integrable and non-integrable) without ever encountering an equilibrium QCP may still give rise to DQPTs in some situations [54, 55]. In an attempt to characterise a DQPT through an order parameter, the crucial role played by topology has been exploited to define a dynamical topological order parameter (DTOP); the DTOP changes its integer value whenever the system dynamically crosses a critical time t_c signalling the occurrence of a DQPT [56].

DQPTs have also been observed for one dimensional systems when the state $|\psi_f\rangle$ is prepared through slow quenching of a parameter of the initial Hamiltonian across QCP(s) [57, 58]. Unlike the sudden quenching case, for slow quenching DQPTs survive in the subsequent evolution following quenches across two QCPs; moreover, the lines of FZs form a lobe like structure in the complex z plane which is also reflected in the temporal evolution of the DTOPs [58]. We note in passing that the study of a slow ramping across a QCP have gained importance because of the possibility of universal Kibble-Zurek scaling [59, 60] of the defect density and the residual energy in the final state reached after the quench [61, 62] (for review see, [26–28]). Generalising to two dimensions, the possibility of the occurrence of DQPTs following a sudden quench from the non-topological phase to the topological phase of the Haldane model [63] and also from the gapped to the gapless phase of a Kitaev honeycomb model have been explored [64]. These studies have shown that in stark contrast to that of the 1D case, the FZs cover areas instead of lines.

We further note that $\text{Re}[f(t)]$ i.e., $(-1/L^d)\text{Re}[\ln \langle \psi_f | e^{-iH_f t} | \psi_f \rangle]$, is closely related to the Loschmidt echo which has been studied extensively close to a QCP both in equilibrium [65–68] and non-equilibrium situations [69–72] and shares a close connection with several other aspects of non-equilibrium dynamics of quenched closed quantum system [73–77]. $\text{Re}[f(t)]$ can also be interpreted as the rate function of the return probability, so called because it can be connected to the singularities in the work distribution function corresponding to zero work following a double quenching process [32].

Very recently, Fläschner *et al.*, [78] has reported the

first experimental observation of a DQPT using time-resolved state tomography to determine the dynamical evolution of a fermionic many-body state after a quench between two lattice Hamiltonians as shall be discussed later in this work. Furthermore, DQPTs have also been investigated in a string of ions simulating interacting transverse-field Ising models in the non-equilibrium dynamics induced by a quantum quench [79]: these transitions have been measured through a quantity that becomes non-analytic in time in the thermodynamic limit.

Consequently, these experiments motivate us, in this paper, to address the possibility of the occurrence of DQPTs following a slow quench of the paradigmatic Haldane model on a hexagonal lattice [80] and investigate the connection between the equilibrium topology of the same model and DQPTs following a slow ramping. We note that the Haldane model has been experimentally realized [81] and for long it has been providing the theoretical base for exploring topological insulators. (In a later experiment, the Chern number of Hofstadter bands with ultracold bosonic atoms was measured [82].) We would like to emphasise at the outset that the focus of this paper is strictly restricted to exploring the role of topology on DQPTs occurring in a quenched Haldane model only and hence, we shall abstain from drawing any parallel to other two dimensional topological or non-topological models. To the best of our knowledge, this is the first attempt to explore the DQPTs following *slow quenches* in a higher dimensional (equilibrium) system which may exhibit effective one-dimensionality in limiting situations. In this work, the (staggered) Semenoff mass term [83] in the topological Haldane model is slowly ramped via a linear quenching protocol with an inverse quenching rate τ so that the system is quenched from one non-topological phase to the other across the topological phase in the process as shown in Fig. 1(a): To observe the DQPTs, one then tracks the LOA of the final state evolving with the time-independent final Hamiltonian. Our study unearths the vital roles played by the parameter τ and more fundamentally, by the Haldane mass in dictating the behavior of FZs and consequently in resultant DQPTs. We note that the slow ramping of the Haldane model has also been studied in the context of inducing topological transitions [84].

Let us summarize our main observations at the outset initially based on the numerical studies of a particular quenching protocol between the same initial and final points, depicted in Fig. 1(a): depending on the inverse quenching rate τ , we observe three distinct behavior of areas of FZs corresponding to a single sector. For very slow ramping, if the rate τ exceeds a critical value, the area of FZs crosses the imaginary z -axis (real time axis) twice. As a consequence, there exist four boundary points of the area those cut the real time axis resulting in four instants of real time where the first derivative of the dynamical free energy shows cusp singularities. For a very rapid quench, on the other hand, the areas do not cross the real axis and there is no DQPT. Notably, we also find

the existence of an intermediate range of τ , separating the no-DQPT region from the re-entrant region, for which the area of FZ cuts the real axis once; as a result, there are only two instants of non-analyticities. Most importantly, the (quasi-momentum dependent) Haldane mass ($M_H(\mathbf{k})$), which makes the Haldane model topologically non-trivial in the phases with non-zero Chern numbers, plays a more fundamental role: $M_H(\mathbf{k})$ is anisotropic in the sense that it is an explicit function of k_x and k_y (i.e., not a function of $|k|$ only) and consequently it leads to the areas of FZs (2D behavior). Furthermore, the critical values of τ (which dictate the cross-over from the no-DQPT region to the intermediate and from the intermediate to the re-entrant region) are determined by the time reversal invariant momentum (TRIM) points of the Brillouin Zone (BZ) (as depicted in Fig. 1(b)) for which $M_H(\mathbf{k}) = 0$. In the situation, when the Haldane mass is altogether absent in the equilibrium model the FZs exhibit an emergent 1D behavior and form lines (*not* areas) which cut the real time axis at specific instants of time leading to non-analyticities in $\text{Re}[f(t)]$ itself: In short, the Haldane mass induces a *dimensional crossover* in the context of DQPTs. In the concluding section, we shall summarise which of the above observations are generic and would hold true for any quenching protocol.

Let us now elaborate on the organization of the paper. In Sec. II, we introduce the Haldane model along

with the quenching protocol emphasizing the role of the Haldane mass. In Sec. III we present and analyze our main results illustrating the behavior of excitation probabilities and the areas of FZs for different values of τ . In Sec. IV, we critically analyze the role of $M_H(\mathbf{k})$ and illustrate how a dense area of FZs emerges from disjoint lines while in Sec. V, we discuss the essential experimental connections. Other than concluding comments presented in Sec. VI, we further include one Appendix, where a brief note on the Haldane model is provided.

II. HALDANE MODEL AND THE QUENCHING SCHEME

Let us consider the 2D topological Haldane model on a hexagonal lattice comprised of two triangular sublattices A and B (refer to Appendix A for detail). The Haldane Hamiltonian is based on a graphene-like Hamiltonian but with a sublattice symmetry (SLS) breaking Semenoff mass (SM) term (M) and a staggered magnetic field which manifests itself in the complex next nearest neighbour hopping. The presence of a periodic boundary condition enables us to write down the Hamiltonian in the quasi-momentum (k_x, k_y) basis as,

$$\mathcal{H}(\mathbf{k}) = \begin{pmatrix} c_A^\dagger(\mathbf{k}) & c_B^\dagger(\mathbf{k}) \end{pmatrix} \begin{pmatrix} h_3(\mathbf{k}) & h_1(\mathbf{k}) + ih_2(\mathbf{k}) \\ h_1(\mathbf{k}) - ih_2(\mathbf{k}) & -h_3(\mathbf{k}) \end{pmatrix} \begin{pmatrix} c_A(\mathbf{k}) \\ c_B(\mathbf{k}) \end{pmatrix}, \quad (1)$$

where $h_3(\mathbf{k}) = M + M_H(\mathbf{k})$ with $M_H(\mathbf{k})$ being the quasi-momentum dependent Haldane mass given by

$$M_H(\mathbf{k}) = 2t_2 \sin(\phi) \left[\sin(\mathbf{k} \cdot \mathbf{a}_2) - \sin(\mathbf{k} \cdot \mathbf{a}_1) + \sin(\mathbf{k} \cdot (\mathbf{a}_1 - \mathbf{a}_2)) \right], \quad (2)$$

that vanishes for $t_2 = 0$ or $\phi = 0$, while

$$h_1 = t_1 \left[1 + \cos(\mathbf{k} \cdot \mathbf{a}_1) + \cos(\mathbf{k} \cdot \mathbf{a}_2) \right] \quad (3)$$

$$h_2 = t_1 \left[\sin(\mathbf{k} \cdot \mathbf{a}_1) + \sin(\mathbf{k} \cdot \mathbf{a}_2) \right], \quad (4)$$

with $\mathbf{a}_1 = \frac{a}{2}(3, \sqrt{3})$ and $\mathbf{a}_2 = \frac{a}{2}(-3, \sqrt{3})$.

We shall henceforth set the lattice constant $a = 1$ and use a rhomboidal BZ as shown in Fig. 1(b). The time reversal symmetry (TRS) in this model is broken by the phase factor ϕ in the Haldane mass term, originating from the staggered magnetic field and is positive for anticlockwise nearest neighbour hopping. The breaking of TRS indicates that the two Dirac points (\mathbf{K} and \mathbf{K}') in bare graphene spectrum are no longer

time-reversed partners of each other as each of them sees a different Haldane mass $M_H(\mathbf{k})$ depending on their quasi-momentum values, i.e., \mathbf{K} or \mathbf{K}' . We will later see that this (Haldane) mass term depends on k_x and k_y explicitly (i.e., does not depend on $|k|$ only), as shown in Fig. 2, and is essential for FZs to cover areas in the complex z plane. For a note on the model (1), we refer to the Appendix A.

We now perform a slow quench on the Haldane model, initially in the ground state $|1_i\rangle$ of the initial Hamiltonian $\mathcal{H}_i(\mathbf{k})$, by linearly ramping the SLS breaking quasi-momentum independent SM term (M) using the protocol $M(t) = -t/\tau$ from an initial value $M_i = 3$ to final value $M_f = -3$ with ϕ fixed to one as illustrated in Fig. 1(a). However, the results presented here would be in general true except for the special situations when $\phi = 0$ and $|M_i|, |M_f| \rightarrow \infty$. In the former case, there is no

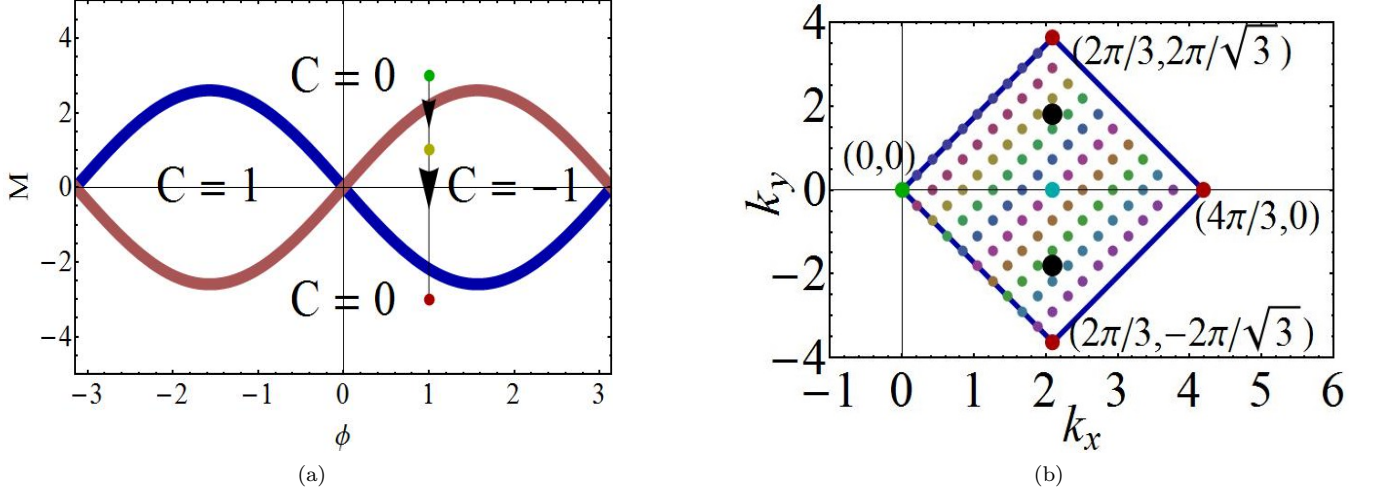


FIG. 1: (a) (Color online) The phase diagram of the Haldane model in $M - \phi$ plane; topological phases and the non-topological phase correspond to Chern numbers $C = \pm 1, 0$, respectively. We employ a quenching scheme $M(t) = -t/\tau$ with $M_i = 3$ (green dot) and $M_f = -3$ (red dot) with $\phi = 1$, so that the system is quenched across both the critical lines (i.e., gapless DPs) in the process of quenching. (One may also consider a slow ramping from $M_i = 3$ (green dot) to $M_f = 1$ (yellow dot).) (b) The rhomboidal Brillouin zone (BZ) that we have chosen in this paper is illustrated for a 10×10 system. The Dirac points are shown in black (biggest dots) while other small dots represent the points of the BZ. The four corner points and the highest symmetry point at the centre (with co-ordinates $(2\pi/3, 0)$) marked by dots of medium size are time reversal invariant momentum (TRIM) points; while the left corner point $(0, 0)$ (in green) and the central point (in cyan) are included in the BZ, other TRIM points (in red) are not. At all TRIM points the Haldane mass is zero.

non-trivial topology of the equilibrium model while the latter situation refers to the infinite time Landau-Zener problem [85, 86] where the role of topology is completely wiped out. In both the cases, we thus arrive at the problem of analyzing DQPTs in a linearly ramped gapped (Semenoff) graphene-like system as elaborated in Sec. IV. Although, the finite time LZ problem can be studied within an analytical framework [87], the results are not useful in the present context and consequently, we shall base our analyses and inferences on extensive numerical calculations of the finite time LZ problem. All these numerical results are analysed and explained using arguments based on symmetry and topology. For the subsequent discussion, we present results for a particular quenching scheme and draw conclusions from them. In the concluding sections, we shall summarise which of these arguments would hold true for the generic situations.

In the process of ramping, the system passes through two gapless critical lines (see Fig. 1(a)) where the characteristic time scale (i.e., the relaxation time) diverges and hence, the condition for an adiabatic dynamics breaks down in their vicinity. One arrives at a final state (for the \mathbf{k} -th mode) at the end of the quenching:

$$|\psi_f(\mathbf{k})\rangle = u_f(\mathbf{k}) |1_f\rangle + v_f(\mathbf{k}) |2_f\rangle, \quad (5)$$

where $|u_f(\mathbf{k})|^2 + |v_f(\mathbf{k})|^2 = 1$, $|1_f\rangle$ and $|2_f\rangle$ are the ground and excited states of the final Hamiltonian $\mathcal{H}(\mathbf{k}, M_f)$ with energy eigenvalues $e_f^1(\mathbf{k})$ and $e_f^2(\mathbf{k})$, re-

spectively; evidently, $|v_{\mathbf{k}}|^2$ stands for the probability of excitation following the ramp and is denoted by $p_{\mathbf{k}}$ in the subsequent discussion.

Thus, the role of the slow quenching process is to prepare the system in the desired final state, $|\psi_f(\mathbf{k})\rangle$ which then evolves in time with the final Hamiltonian ($\mathcal{H}_f(\mathbf{k})$) yielding $e^{-i\mathcal{H}_f(\mathbf{k})t'} |\psi_f(\mathbf{k})\rangle$, where $t' = t - t_f$ is measured from the instant when the final state is attained. One then immediately finds the LOA, $G(t') = \prod_{\mathbf{k}} \langle \psi_f(\mathbf{k}) | e^{-i\mathcal{H}_f(\mathbf{k})t'} | \psi_f(\mathbf{k}) \rangle$, which contains contribution from all the quasi-momenta (\mathbf{k}) modes. Thus, to clarify, there are two kinds of evolution, one that takes $|1_i\rangle$ at initial time $t_i = 0$ to final quenching time $t = t_f$ using the protocol $M(t) = -t/\tau$, to reach the state $|\psi_f\rangle$, which then evolves with time-independent $\mathcal{H}_f(\mathbf{k})$.

Moving on to the complex z -plane, we now solve for the zeros of the dynamical partition function (FZs) ($G(z) = 0$) to locate the dynamical critical points. It is then straightforward to show that the FZs are given by,

$$z_n(\mathbf{k}) = \frac{1}{e_f^2(\mathbf{k}) - e_f^1(\mathbf{k})} \left[\log \left(\frac{p_{\mathbf{k}}}{1 - p_{\mathbf{k}}} \right) + i\pi(2n+1) \right] \quad (6)$$

where $n = 0, \pm 1, \pm 2, \dots$ are integers; a particular value of n corresponds to one set of FZs and we shall essentially focus on the $n = 0$ sector. It should however be noted that although the equation for FZs in Eq. (6) have similar form as in the sudden quenching case [32, 63], the excitations probabilities $p_{\mathbf{k}}$ in the present case are determined by the ramping protocol. We reiterate that these excitation probabilities are numerically

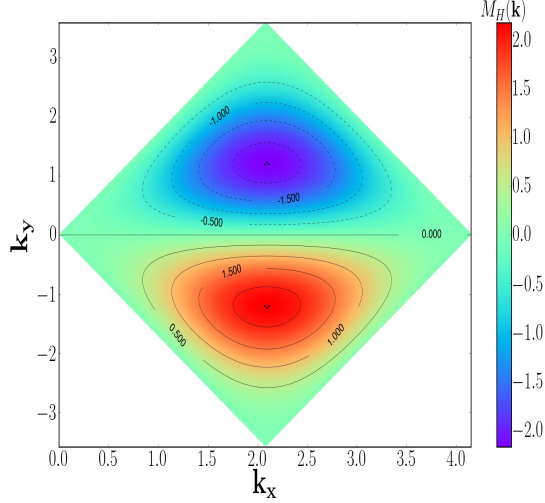


FIG. 2: The variation of the Haldane mass $M_H(\mathbf{k})$ in the Brillouin zone (BZ) as a function of k_x and k_y . It is zero along the k_x axis when $k_y = 0$ while it is positive (negative) in the lower (upper) half-plane. As a consequence of the time reversal invariance of this mode, M_H vanishes at all the TRIM points. Following any contour of fixed $M_H(\mathbf{k})$ in the BZ, one can immediately conclude that the Haldane mass must explicitly depend on k_x and k_y and not $|k|$ only.

estimated through a finite LZ problem for each mode \mathbf{k} . The particle-hole symmetric nature of the Haldane Hamiltonian (1) demands that $e_f^2(\mathbf{k}) = -e_f^1(\mathbf{k})$, yielding

$$z_n(\mathbf{k}) = \frac{1}{2e_f^2(\mathbf{k})} \left[\log \left(\frac{p_{\mathbf{k}}}{1 - p_{\mathbf{k}}} \right) \right] + i\pi(2n + 1). \quad (7)$$

These FZs when plotted in the complex z -plane for each value of k_x and k_y (for a fixed n) may come together to form a line or cover a dense area depending upon the effective dimension of the system. Substituting $p_{\mathbf{k}} = 1/2$ for the mode $\mathbf{k} = \mathbf{k}^*$, in Eq. (6) renders the real part of z_n zero while the imaginary part is given by $i\pi(2n + 1)/2e_f^2(\mathbf{k}^*) = it_c$; at these instants of real time,

$$t_c^{(n)} = \frac{\pi(n + \frac{1}{2})}{e_f^2(\mathbf{k}^*)} \quad (8)$$

one observes DQPTs, namely the non-analyticities (cusp singularities) in $\text{Re}(f(t))$ or $\text{Re}(f'(t))$ with the critical times ($t_c^{(n)}$) being inversely proportional to the energy (of the excited state) $e_f^2(\mathbf{k}^*)$ of H_f . We also note that given the two-level nature of the problem the condition $p_{\mathbf{k}^*} = 1/2$ implies an effective infinite temperature state of the final Hamiltonian for the mode \mathbf{k}^* . For brevity, we shall henceforth drop the subscript f in $e_f^2(\mathbf{k})$.

Let us now illustrate how the presence of a non-zero $M_H(\mathbf{k})$ is essential in resulting in dense areas of FZs in the complex z plane. Given the two-dimensional nature of the Haldane Hamiltonian, one naturally expects that

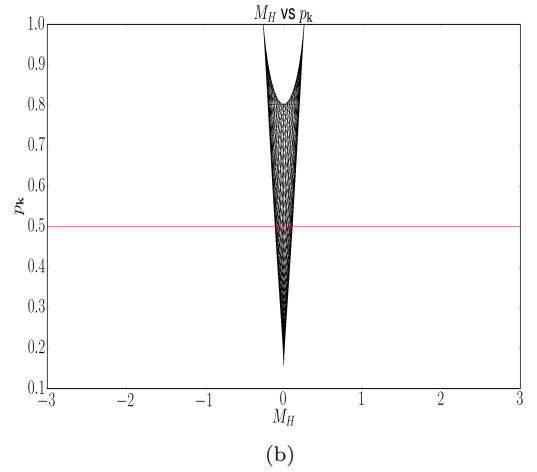
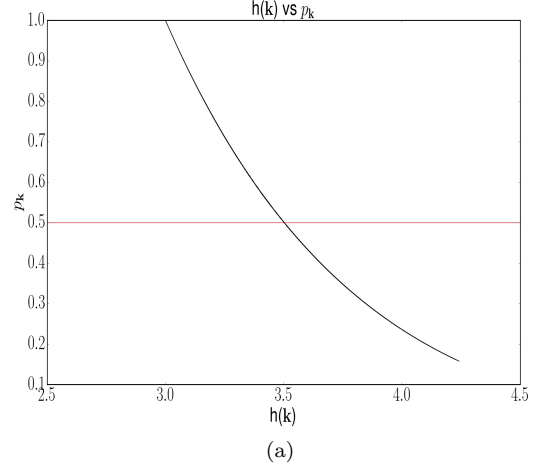


FIG. 3: (Color online) (a) The variation of $p_{\mathbf{k}}$ with $h(\mathbf{k}) = \sqrt{h_1^2(\mathbf{k}) + h_2^2(\mathbf{k}) + M_f^2}$, has been plotted for a quench from $M_i = 3$ to $M_f = -3$ with a $\tau = 0.1$ for a small $\phi = 0.1$. The $p_{\mathbf{k}^*} = 1/2$ (in red) line intersects with the curve at only one point indicating that all \mathbf{k}^* 's lead to the same value of $h(\mathbf{k}^*)$. (b) The multiple intersections of the $p_{\mathbf{k}^*} = 1/2$ line in the plot of $p_{\mathbf{k}}$ vs M_H shows that different \mathbf{k}^* 's yield different contributions to $e_f^2(\mathbf{k}^*)$ rendering it anisotropic, thereby leading to a continuum of critical t_c 's.

the values of k_x, k_y with the same excitation probability $p_{\mathbf{k}}$ must lie within a continuum band or range. It is now important to analyze whether these particular values of \mathbf{k} for the entire range correspond to the same value of $e^2(\mathbf{k})$; otherwise, Eq. (7) (for a given n) ensures that the FZs corresponding to all these modes must lie at different points in the complex z -plane.

Referring to the Hamiltonian (1), we find that $e^2(\mathbf{k}) = \sqrt{(h_1^2(\mathbf{k}) + h_2^2(\mathbf{k}) + [M_f + M_H(\mathbf{k})]^2)}$. We note that the contribution to energy $e^2(\mathbf{k})$ from $(h_1^2(\mathbf{k}^*) + h_2^2(\mathbf{k}^*) + M_f^2)$ for the values of \mathbf{k}^* 's for which $p_{\mathbf{k}^*} = 1/2$ are all the same as is apparent from the Fig. 3(a); this figure shows that the " $p_{\mathbf{k}^*} = 1/2$ " line intersects only at one point

with the $p_{\mathbf{k}}$ vs $h(\mathbf{k}) = \sqrt{h_1^2(\mathbf{k}) + h_2^2(\mathbf{k}) + M_f^2}$ curve. Consequently, it turns out to be absolutely necessary to explore the variation of M_H across the BZ to conclude about the functional dependence of $e^2(\mathbf{k})$ on k_x and k_y . From Fig. 2, we immediately conclude that $M_H(\mathbf{k})$ is anisotropic in k_x and k_y and has an explicit functional dependence on them. Now focussing on Fig. 3(b), we observe that even when the Haldane mass is quite small with $\phi = 0.1$, we see that the $p_{\mathbf{k}^*} = 1/2$ line passes through a set of points corresponding to different values of $M_H(\mathbf{k}^*)$. Therefore, such a dependence makes $e^2(\mathbf{k})$ depend explicitly on k_x and k_y and hence FZs with different \mathbf{k} (corresponding to the same $p_{\mathbf{k}}$) would lie at different points in the complex z -plane, resulting in an area of FZs for a particular n . Further, from Eq. (8), we then conclude that FZs corresponding to different \mathbf{k}^* must touch the real time axis (imaginary z -axis) at different instants. Although the result presented in Fig. 3 is plotted for a particular quenching scheme ensuring that \mathbf{k}^* exists, this needs to be emphasised that the fact that the anisotropic continuous variation of the Haldane mass is at the root of generating areas in the complex z -plane holds true for any quenching protocol (sudden or slow) and any set of parameter values and even when \mathbf{k}^* may not exist. On the contrary, when $M_H(\mathbf{k}) = 0$ in the equilibrium model, this explicit dependence on k_x and k_y disappears, as is evident from Fig. 3(a), and one gets an effective one-dimensional behavior where one observes lines of FZs, (*not* areas). This issue will be further elaborated in Sec. IV.

III. RESULTS AND ANALYSES

In this section we present the main results of our paper based on the quenching scheme $M(t) = -t/\tau$ with $M_i = 3$ and $M_f = -3$ with $\phi = 1$ as shown in Fig. 1(a) and discuss three cases which illustrate how the appearance of FZs vary with the inverse rate of quenching τ as we tune it from the sudden limit (when $\tau \rightarrow 0$) to the extreme slow limit (when $\tau \rightarrow \infty$) ramping the system linearly across two massless DPs (see Fig. 4).

As is evident from the figures in all situations $p_{\mathbf{k}}$ is 1 at the DPs and smaller than 1 for modes away from them. Consequently, from Eq. (7), we conclude that FZs corresponding to DPs would tend to $+\infty$, while for the modes with $p_{\mathbf{k}} \rightarrow 0$ the FZs would approach $-\infty$, yielding the possibility of FZs extending from $-\infty$ to $+\infty$ in the thermodynamic limit. We note that the maximum value of $p_{\mathbf{k}}$ is of the order of .999 (i.e., nearly unity) near the DPs ensuring that our numerical scheme is significantly accurate.

Let us first consider the extreme limit, i.e., the sudden quenching limit where the value of $\tau \rightarrow 0$. Therefore, although the system is quenched across both the QCPs, as shown in Fig. 4(a), the rapid rate of quenching never allows the minimum value of $p_{\mathbf{k}^*}$ to become less than $1/2$; consequently, area of FZs never cross the real

time axis (as shown in Fig. 4(b)) and hence there is no non-analyticity either in $\text{Re}[f(t)]$ or in its time derivative resulting in a complete absence of DQPTs.

Now considering the other extreme limit, i.e., the slow limit (see Fig. 4(c)), let us follow the contour plot of the excitation probability, $p_{\mathbf{k}}$ along the $k_x = \frac{2\pi}{3}$ line. Every time the system goes from a value of $p_{\mathbf{k}} = 0$ to $p_{\mathbf{k}} = 1$, the excitation probability attains the value of $p_{\mathbf{k}} = p_{\mathbf{k}^*} = 1/2$. These values of k_x^* and k_y^* form two lobes (closed contours) of $p_{\mathbf{k}^*} = 1/2$ centred around the two DPs. Referring to Eq. (6) and the discussion following it, one can explain the observation, as shown in Fig. 4(d), that the area of FZs (for $n = 0$) crosses the real time axis twice which means that their boundaries cross four times; this behavior of the areas of FZs is referred to as re-entrances. Referring to the inset of Fig. 4(d), the line $p_{\mathbf{k}^*} = \frac{1}{2}$ cuts the area generated by $e^2(\mathbf{k})$ multiple times leading to a continuum band or range of \mathbf{k}^* with four boundary values of $e^2(\mathbf{k}^*)$; these boundary values when substituted in Eq. (8) (with $n = 0$) lead to four time scales t_b^1 , t_e^1 , t_b^2 and t_e^2 , corresponding to upper and lower lobes of $p_{\mathbf{k}^*} = 1/2$ contours. Consequently, $\text{Re}[f'(t)]$ shows cusp singularities at these instants of time (see Fig. 5(a)). Again, from Eq. (8), we immediately conclude that t_b^1 and t_b^2 corresponds to the maximum of the highest and the lowest energy bands, while t_e^1 and t_e^2 are given in terms of the minimum of these two energy bands.

Focussing on the $n = 0$ sector, we have so far analysed two limits of τ : extreme fast ($\tau < \tau_1^c$), when there is no DPT and the extreme slow ($\tau > \tau_2^c$) when there are re-entrances. But the most intriguing situation arises at intermediate values of $\tau = \tau_i$, where $\tau_1^c < \tau_i < \tau_2^c$. Here, although the system passes through two critical points, the FZs (for $n = 0$) collate to form an area in the complex z plane whose boundaries cross the real time axis at two pairs of time instants only (see Fig. 4(f)), in stark contrast with re-entrance of FZs shown in Fig. 4(d). Carefully analysing this scenario from Fig. 4(e), we note that the crucial difference with the re-entrance case happens to be the fact that there exists only a *single* $p_{\mathbf{k}} = p_{\mathbf{k}^*} = 1/2$, curve encircling both the DPs (QCPs). Focusing on the variation of $p_{\mathbf{k}} = 1/2$ with k_y on the line $k_x = 2\pi/3$, we conclude that $p_{\mathbf{k}}$ gradually becomes smaller than $1/2$ with distance from DPs on either side (of the DPs) but is definitely greater than $1/2$ between them. The upper critical value τ_2^c is that value of τ_i for which the $p_{\mathbf{k}}$ becomes $1/2$ between the two DPs on the $k_x = 2\pi/3$ line at the point $k_y = 0$: for $\tau > \tau_2^c$, we see the formation of two $p_{\mathbf{k}} = p_{\mathbf{k}^*} = 1/2$ contours encircling the two DPs emerging from the single contour for $\tau < \tau_2^c$. Therefore, in the intermediate regime, the value of τ_i is such that there is only one $p_{\mathbf{k}} = p_{\mathbf{k}^*} = 1/2$ lobe enclosing the two DPs resulting in the creation of a single area of FZs. Once again, recalling Eq. (8), the lower (upper) boundary of the area that crosses the real time axis is determined by the maximum (minimum) of $e^2(\mathbf{k})$ on the line $p_{\mathbf{k}} = 1/2$ (inset of Fig. 4(f)) and one observes cusp singularities in $\text{Re}[f'(t)]$ only at two instants of real time

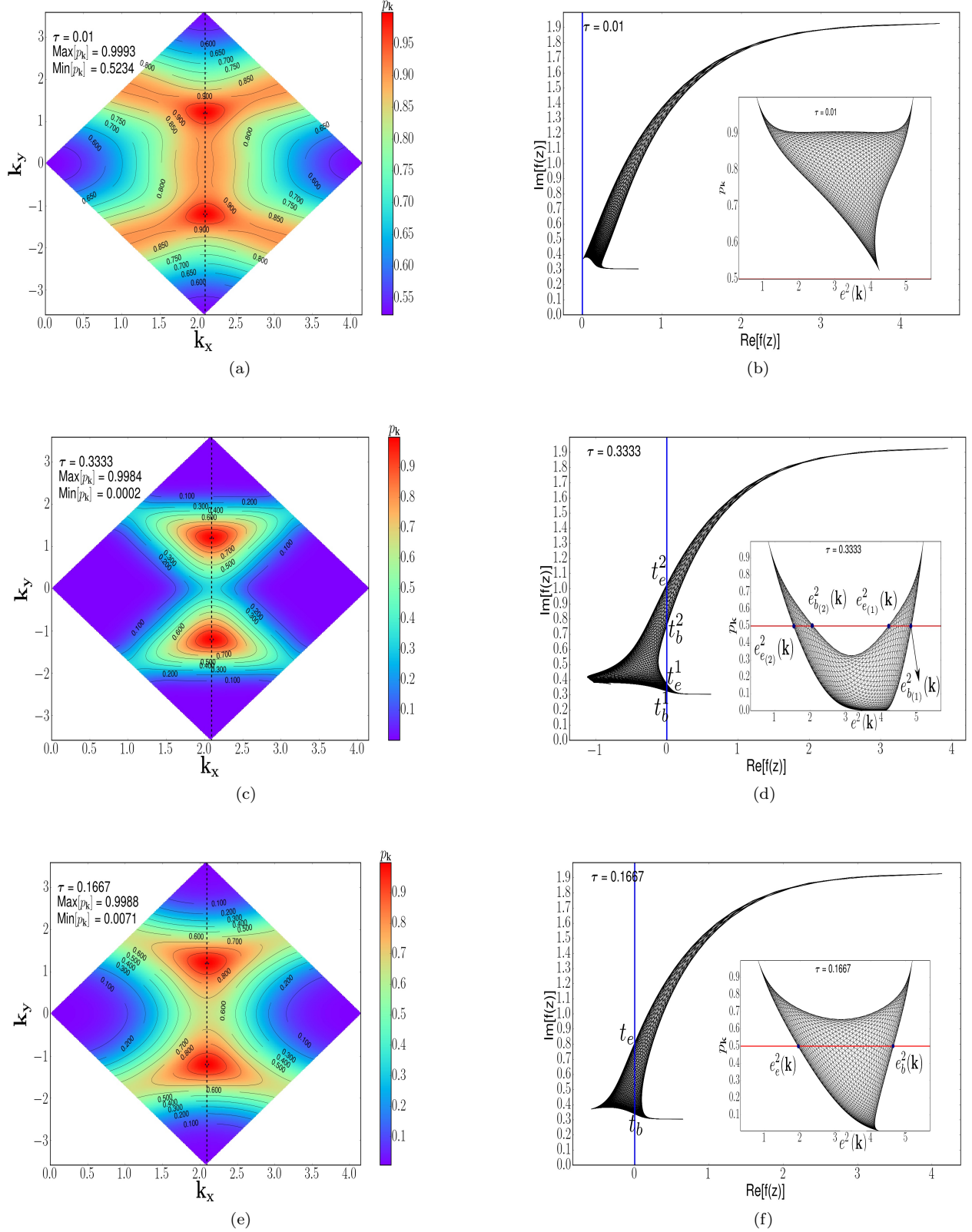


FIG. 4: (color online) This set of figures presents the variation of $p_{\mathbf{k}}$ in the $k_x - k_y$ plane and no-DQPT, re-entrant and intermediate behaviours of FZs for the sector $n = 0$ with $M_i = 3, M_f = -3, \phi = 1$ and $L = 100$. In Figs. 4(a) and 4(b), τ is small ($< \tau_c^1$) so that the minimum value of $p_{\mathbf{k}} \geq 1/2$ for all values of \mathbf{k} and the area never crosses the real axis. The inset of Fig. 4(b), validates the observation that there is no DQPT by showing that the area formed by $e^2(\mathbf{k})$ does not touch the line $p_{\mathbf{k}} = p_{\mathbf{k}^*} = 1/2$ for any value of the \mathbf{k} . On the contrary, Fig. 4(c) shows that in the extreme slow limit, i.e., $\tau > \tau_c^2$, $p_{\mathbf{k}}$ becomes less than $1/2$ along the dotted line connecting two DPs and there is a re-entrant behavior of FZs evident in Fig. 4(d): the inset shows four boundary points of $e^2(\mathbf{k})$ on the line $p_{\mathbf{k}^*} = 1/2$ leading to four instants of time t_b^1, t_e^1, t_b^2 and t_e^2 , (as obtained from Eq. (8)) where $\text{Re}[f'(t')]$ is non-analytic (see Fig. 5(a)). For $\tau_1^c < \tau < \tau_c^2$, Fig. 4(e) shows that $p_{\mathbf{k}}$ never becomes less than $1/2$ along the dotted line and consequently, the area of FZs cross the real time axis only once (Fig. 4(f)): the inset shows the boundary points those lead to t_b and t_e , where $\text{Re}[f'(t')]$ is non-analytic as shown in Fig. 5(b)).

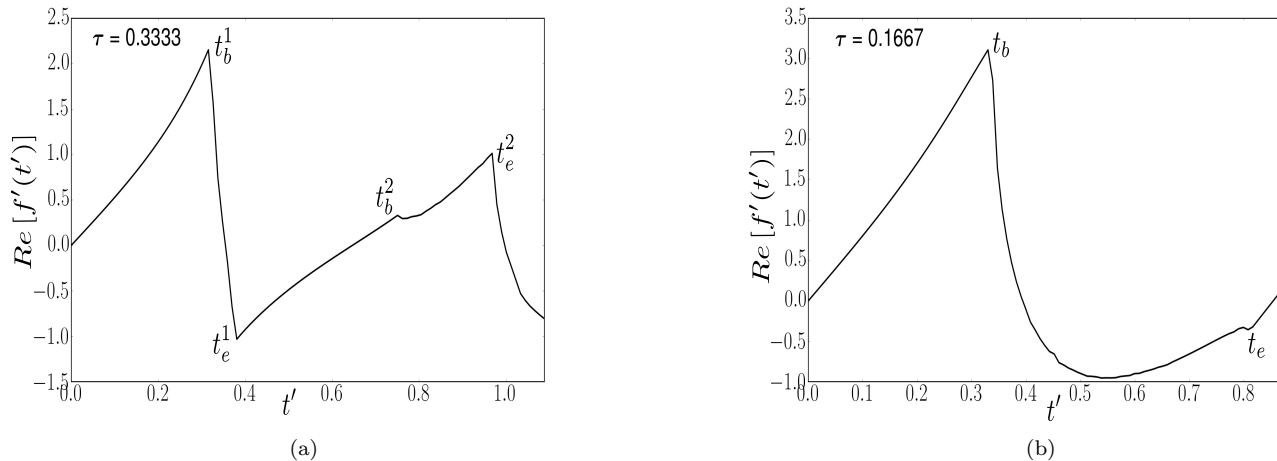


FIG. 5: The non-analyticities (cusp singularities) in $\text{Re}[f'(t')]$ in the re-entrant and the intermediate situations (as predicted in Figs. 4(c)-4(f)) are shown in Figs. 5(a) and 5(b), respectively, for $n = 0$. Here, although we have used same τ , ϕ , M_i and M_f values as in Fig. 4, L is chosen to be 1000 to accentuate the instants of real time at which sharp non-analyticities appear.

as shown in Fig. 5(b).

The question that naturally arises at this point is what determines the crossover values of the rate τ for which the transitions between the three different regions occur and how do these scales depend on the parameter ϕ (or specifically M_H). Recalling the fact that the $p_{\mathbf{k}}$ is the smallest for the modes corresponding to the left corner TRIM point at $k_x = k_y = 0$ fully included in the BZ as shown in Fig. 1(b), we focus on this TRIM point. Since the minimum value of $p_{\mathbf{k}}$ must at least be $1/2$ for DQPTs to appear, the condition $\text{Min}[p_{\mathbf{k}}] = 1/2$, at this corner TRIM point determines the scale τ_c^1 as shown in Fig. 6(a). $\text{Min}[p_{\mathbf{k}}]$ at this TRIM, is independent of M_H , and evidently so is τ_c^1 .

On the other hand, the transition from the intermediate to the re-entrant phase taking place at τ_c^2 occurs when the $p_{\mathbf{k}} = 1/2$ lobe enclosing the two DPs separate out at the other TRIM point $k_x = 2\pi/3, k_y = 0$ (located at the centre of BZ) with zero Haldane mass, to form two distinct lobes enclosing one DP each (Fig. 6(c)). When the value of τ is insufficient to make the $p_{\mathbf{k}}$ at this mode less than $1/2$, the system remains in the intermediate phase, but at $\tau = \tau_c^2$, $p_{\mathbf{k}}$ becomes $1/2$ at this mode and the system enters the re-entrant phase for $\tau > \tau_c^2$. Hence, this mode being independent of M_H again keeps τ_c^2 invariant under the variation of ϕ . We further emphasize that both τ_c^1 and τ_c^2 are determined by TRIM points, and hence, are independent of the system size as long as it is ensured that the numerical scheme sharply includes these points while enumerating different modes of the BZ. Of course, these critical values do not get altered in the thermodynamic limit.

Having established the independence of τ_c^1 and τ_c^2 on the parameter ϕ (though they indeed depend on M_i , M_f), we shall now proceed to argue how the area of FZs (for the sector $n = 0$) should look at these critical

rates $\tau = \tau_c^1$ and τ_c^2 . Note that at $\tau = \tau_c^1$, $p_{\mathbf{k}}$ corresponding to the mode $k_x = 0, k_y = 0$ becomes $1/2$ and it is *only* the FZ corresponding to this particular point of the area which touches the real time axis as shown in Fig. 6(b). On the contrary, at $\tau = \tau_c^2$, the internal boundary of the area of FZs touches the real axis for the mode $k_x = 2\pi/3, k_y = 0$, in addition to already existing two crossings due to the intermediate behaviour. In short, the area crosses the real time axis for two momenta and additionally touches it for the above TRIM point (Fig. 6(d)). When τ exceed τ_c^1 (τ_c^2) even infinitesimally, the intermediate (re-entrant) behaviour as shown in Figs. 4(c)-4(f) sets in.

IV. LIMITING SITUATIONS: FORMATION OF AREAS OF FZS DUE TO $M_H(\mathbf{k})$

We have already demonstrated that the non-zero Haldane mass plays a crucial role in generating areas of FZs in the complex z plane. Furthermore, it vanishes for the TRIM points which determine the characteristic values of τ , i.e., τ_c^1 and τ_c^2 . In this section, we shall revisit the crucial role played by $M_H(\mathbf{k})$ by considering some limiting situations. Let us first analyze the situation when the Haldane mass altogether vanishes, (i.e., the parameter $\phi = 0$) so that the equilibrium model is simply a massive Dirac Hamiltonian which does not possess any non-trivial topology (see Fig. 7). This model is well studied and known to mimic the graphene Hamiltonian on a Boron Nitride substrate. Although the results presented Fig. 7 are obtained for the lattice model i.e., Eq. (A1) with $t_2 = 0$, to get an intuitive understanding of the results, we resort to the low-energy continuum limit: one can then recast the Hamiltonian (1) in the vicinity of DPs with $M_H(\mathbf{k}) = 0$, in the form:

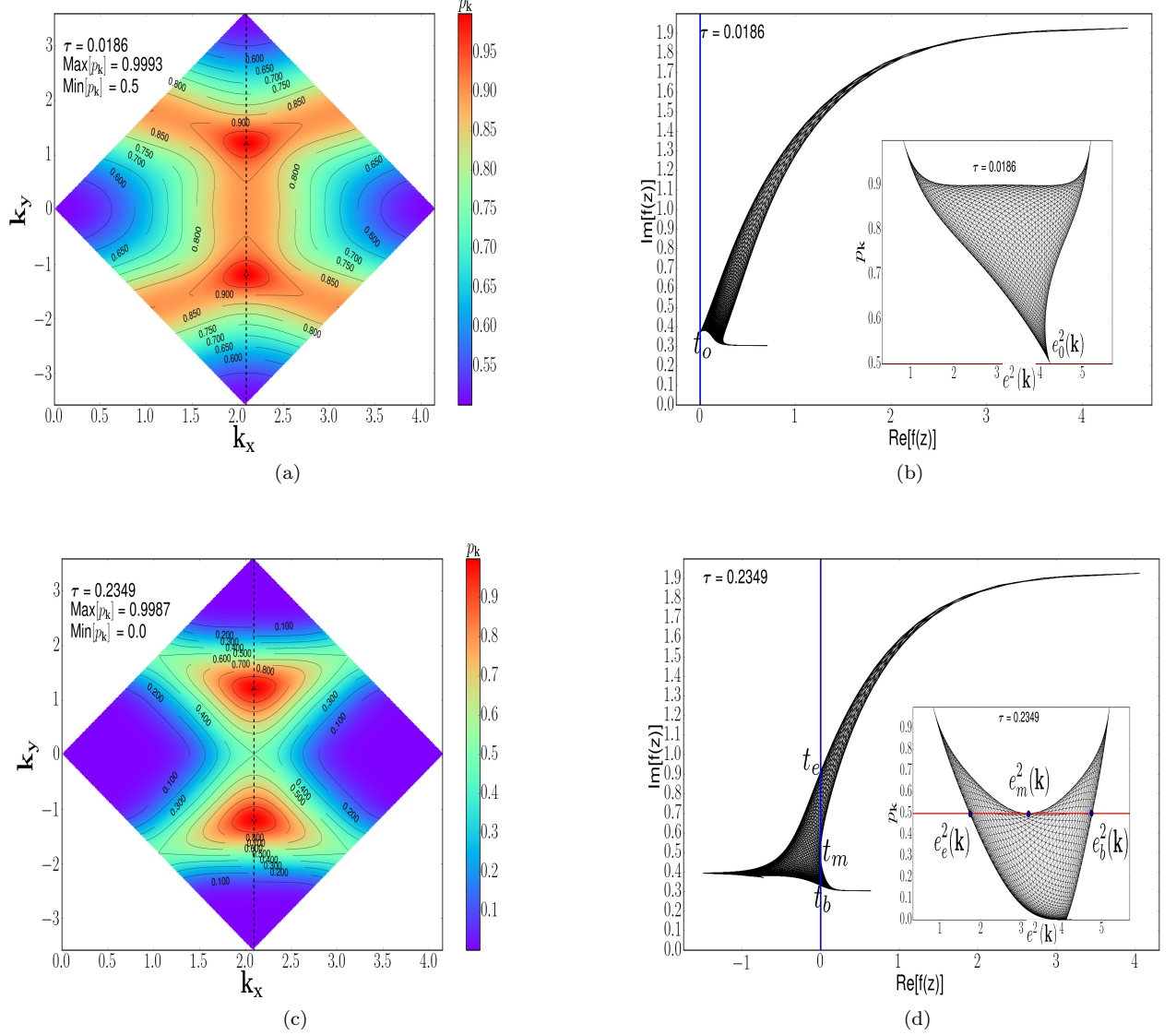


FIG. 6: (color online) This set of figures presents the scenario occurring at the critical values of τ , namely, τ_c^1 and τ_c^2 , with $M_i = 3, M_f = -3, \phi = 1$ and $L = 100$. As shown in Fig. 6(a), at $\tau = \tau_c^1$, the excitation probability $p_{\mathbf{k}}$ becomes 1/2 for the mode $k_x = k_y = 0$ (the TRIM point at the corner of BZ in Fig. 1(b)) for which $M_H = 0$. Fig. 6(b) shows that the area of FZs touch the imaginary (real time) axis for this mode at the instant t_m ; the inset shows that $e^2(\mathbf{k})$ touches the $p_{\mathbf{k}} = 1/2$ line for this momentum mode. On the contrary, at $\tau = \tau_c^2$ (Fig. 6(c)), $p_{\mathbf{k}}$ just becomes 1/2 for the TRIM point at the centre of the BZ. Consequently, as shown in (Fig. 6(d)), the internal boundary of the area of FZs touches the real time axis for this mode; this is more transparently depicted in the inset, there is an additional boundary point for the energy $e_m^2(\mathbf{k})$ (that corresponds to the instant t_m) when compared to the inset of the Fig. 4(f).

$$\mathcal{H} = \begin{pmatrix} M(t) & k_x + ik_y \\ k_x - ik_y & -M(t) \end{pmatrix}, \quad (9)$$

where k_x, k_y are measured from each DP. The SM, $M(t) = -t/\tau$ is ramped from $M_i = +3$ to $M_f = -3$ as shown in 1(a) but with $\phi = 0$; the system is thus quenched through two gapless DPs, which, in the present case, are time reversed partners of each other). Although

referring to Fig. 7(a), we find $p_{\mathbf{k}} = 1$ at both DPs, FZs (for the sector with $n = 0$) form a single line in the z -plane (Fig. 7(b)) cutting the real time axis only once; the re-entrant behavior observed in Fig. 4(d) also completely disappears because the lines of FZs associated with the upper and lower DPs fall on top of each other coalescing into the observed single line.

To comprehend this observation, let us note in the present case, one can argue that the modes \mathbf{k}^* (for which

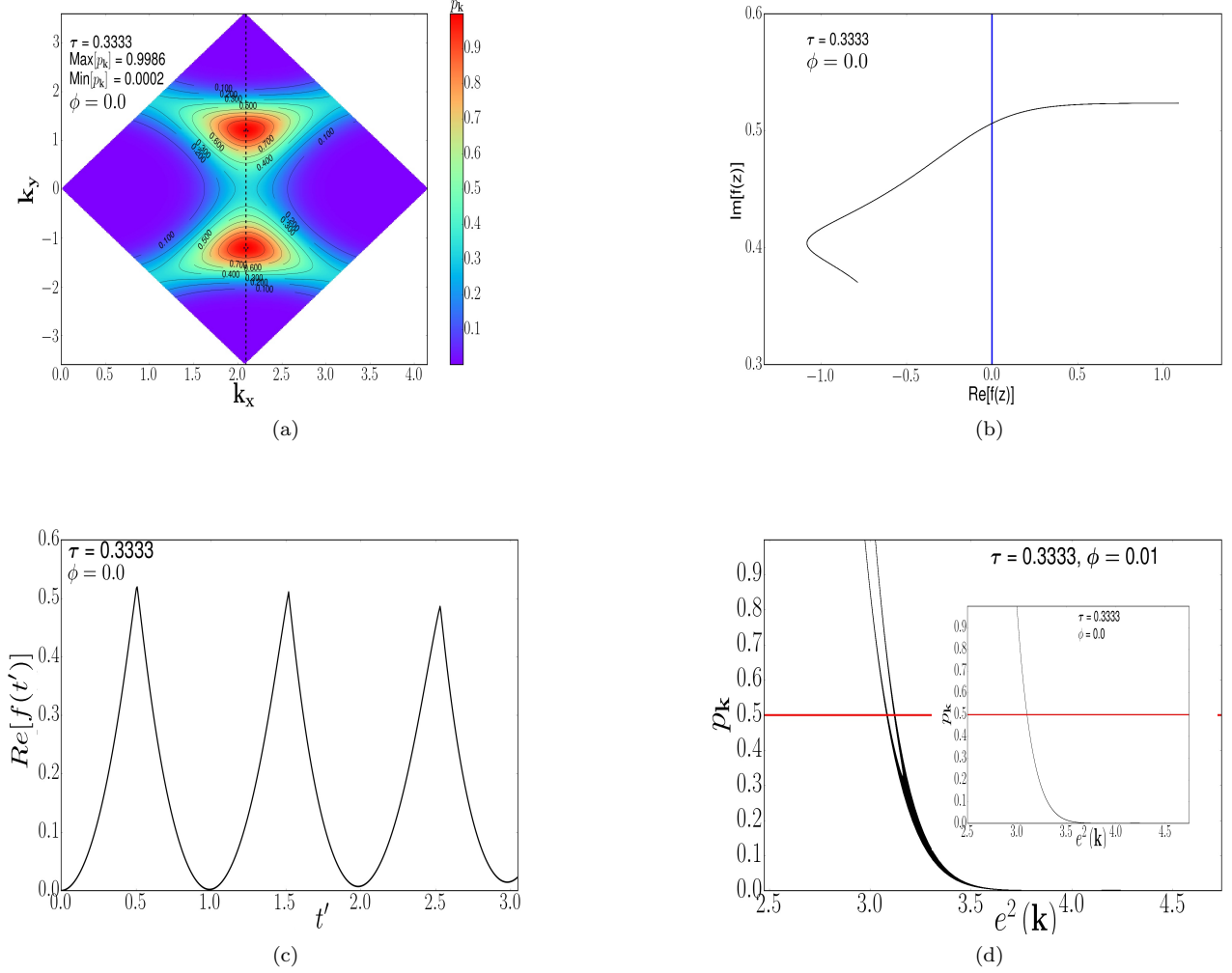


FIG. 7: (color online) These figures demonstrate the effective 1D behavior that emerges when the parameter ϕ and consequently, M_H vanishes; we choose $\tau = .3333$, so that for $\phi \neq 0$, there is a re-entrant behavior as presented Figs. 4(c) and 4(d). Fig. 7(a) shows that the excitation probability $p_{\mathbf{k}} \sim 1$, around both the DPs. Nevertheless, as shown in Fig. 7(b), the FZs constitute a line rather than an area; furthermore, the re-entrant behavior completely disappears. As elaborated in the text, in Fig. 7(c), we show that there exist sharp non-analyticities in $\text{Re}[f(t)]$ itself at different instants of time and we choose $n = 0, 1$ and 2 . In Fig. 7(d), it is illustrated that even for very small ϕ , there are four boundary points of $e^2(\mathbf{k})$ on the line $p_{\mathbf{k}^*} = 1/2$, which shrink to one point as soon as ϕ vanishes (inset).

$p_{\mathbf{k}^*} = 1/2$), satisfy the condition $|\mathbf{k}^*|^2 = (k_x^*)^2 + (k_y^*)^2 =$ constant. More importantly, $e^2(\mathbf{k}) = \sqrt{|\mathbf{k}|^2 + M_f^2}$ is no longer anisotropic, rather depends only on $|\mathbf{k}|$. Evidently, the entire range of \mathbf{k}^* leads to the same value of $e^2(\mathbf{k}^*)$. Consequently, the system is effectively one-dimensional. of real time (for each n) at which $\text{Re}[f(t)]$ itself shows a cusp singularity, as presented in Fig. 7(c), with a discontinuous change in its first derivative. Even for an infinitesimally small ϕ , the areas of FZs reappear along with the re-entrant behavior (Fig. 7(d)).

Let us now extend to the situation when the Haldane mass is $M_H^\alpha(\mathbf{k})$ in the continuum limit is positive at one DP and negative at the other. Expanding around these DPs labelled by the index $\alpha = \pm 1$, we arrive at two

Hamiltonians:

$$\mathcal{H}^\alpha = \begin{pmatrix} M(t) + M_H^\alpha & k_x + ik_y \\ k_x - ik_y & -(M(t) + M_H^\alpha) \end{pmatrix}, \quad (10)$$

where the Haldane mass $M_H = -3t_2\alpha \sin \phi$. In this case, though M_H is independent of the magnitude of the quasi-momentum, the two DPs sense different M_H . This is reflected in the behavior of FZs, which now form two disjoint lines corresponding to the sector $n = 0$ as shown in Fig. 8(a), which cut the real axis at two different instants of time. We emphasise that an area of FZs does not appear in this case and at the same time, there is a deviation from the one dimensional situation depicted in Fig. 7(b).

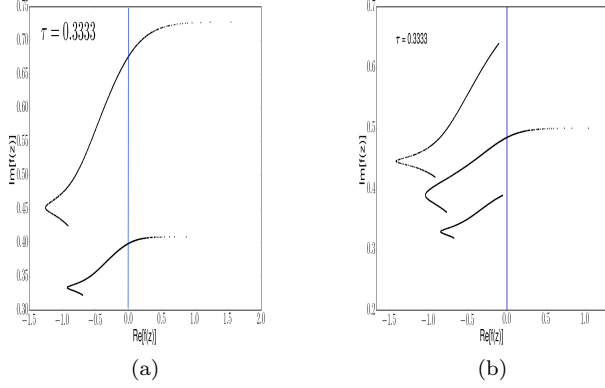


FIG. 8: (a) The FZs when $M_H(\mathbf{k})$ assumes two constant values (with different signs) at two DPs; we obtain two disjoint lines of FZs both crossing the real time axis at two different instants. (b) This refers to a hypothetical situation where the Haldane mass assumes three constant values in three regions of the BZ as elaborated in the text and consequently one obtains three disjoint lines.

The continuum limit discussed above can also be viewed as a special situation where M_H is positive in the upper half of the BZ while negative in the lower half. This can be further extended to an artificial situation where M_H assumes three different values along three regions parallel to the k_x -axis of the BZ where the central region extends from $k_y = \pi/\sqrt{3}$ to $k_y = -\pi/\sqrt{3}$ with a constant Haldane mass M_H^2 , whereas the regions above and below it have constant masses M_H^1 and M_H^3 , respectively, with the condition $M_H^1 > M_H^2 > M_H^3$ so that the topological structure presented in the Fig. 1(a) remain intact. In this case, one finds three disjoint lines of FZs as shown in Fig. 8(b). When generalized to n similar stripes with constant mass $M_H^{(n)}$ for the n -th stripe, more and more disjoint lines of FZs appear. Equipped with this important observation, one can now view the continuous variation of the $M_H(\mathbf{k})$ across the BZ (Fig. 2), as a limiting situation when area of these regions becomes infinitesimal; in a such scenario these disjoint lines coalesce to form a quasi-area which becomes a real dense area in the thermodynamic limit. This provides an intuitive explanation of how the anisotropy in $M_H(\mathbf{k})$ generates areas of FZ from otherwise disjoint lines. In short, there is a deviation from the emergent one-dimensional behavior as soon as the topological mass term is incorporated in any form using discrete variations over the BZ so that the topological structure remains invariant; corresponding disjoint lines of FZs (of the same sector) coalesce to form an area in the limit when the Haldane mass is allowed to vary continuously over the BZ as happens in the lattice version of the model (A1).

V. EXPERIMENTAL CONNECTIONS

Jotzu *et al.* [81] demonstrated that the experimental realisation of the Haldane Hamiltonian is indeed possible with ultracold atoms in optical lattices periodically modulated in time. A rotating force, as proposed by Oka and Aoki [13], in a honeycomb lattice breaks TRS and leads to the necessary complex next-neighbor hopping giving rise to a Floquet Hamiltonian with Haldane-like mass term. In the above mentioned experiment [81], a honeycomb optical lattice, was created by several laser beams arranged in the $x - y$ plane, which generates the hopping terms h_1 and h_2 in Eq. (1), and the atoms in A and B sublattices were separated via a large offset (or the SM denoted by M in h_3 of Eq. (1)), which can be tuned by changing the polarisation of the laser. The lowest band was then filled with non-interacting, ultracold gas of fermionic ^{40}K atoms before ramping up a sinusoidal modulation of the lattice position along the x and y directions which resulted in TRS preserving linear ($\phi = 0, \pi, 2\pi$), and TRS breaking circular ($\phi = \pi/2$) and elliptical ($\phi \neq 0, \pi/2, \pi, 2\pi$) Haldane-like mass term M_H given in the Haldane Hamiltonian. Later, Flaschner *et al.* [78] using a similar setup studied the time evolution of fermionic quantum gases in such a hexagonal optical lattice after a rapid quench from a topologically trivial system into a Haldane-like system by quenching between a static and a Floquet Hamiltonian which generates the dynamics. The initial many-body ground state is a band insulating state in the lowest band of such a hexagonal lattice with a large offset between the A and B sites. A quench into the final Floquet Hamiltonian (manifested through resonant circular lattice shaking) was then performed. Finally, a momentum and time-resolved state tomography measured this out of equilibrium dynamics after the stroboscopic evolution times of the Floquet Hamiltonian, yielding the evolution of the many-body state on the Bloch sphere, thereby, ascertaining the occurrence of DQPTs. Similarly, a slow ramping instead of a rapid quench into the final Floquet Hamiltonian seems plausible and may indeed corroborate our results. It should also be noted that the finite time LZ limit, on which we focus on, is more feasible to experimental verification than an infinite LZ limit. Furthermore, there has also been a recent work in which Yang-Lee zeros have been observed experimentally [88].

VI. CONCLUSION

Exploiting the two band nature of the topological Haldane model which enables us to employ extensive investigations of finite time LZ problems, we establish a deep connection between the equilibrium topology of the Haldane model and subsequent DQPTs following a linear ramping of the SM from one non-topological phase to the other. Other than the re-entrance of areas of FZs in the extreme slow limit which is an artefact of quenching

across two DPs, we establish the existence of an intermediate range of the quenching rate for which areas of FZs cross the real axis only once leading to two (instead of four as in the re-entrant case) instants of non-analyticities in $\text{Re}[f(t')]$ for a fixed value of n . This intermediate region, which do not show up in the case of the transverse Ising chain [58], exists only because of the position of the DPs inside the BZ; this allows $p_{\mathbf{k}}$ to vanish above (below) the upper (lower) DP along the line $k_y = 2\pi/3$ while keeping it always greater than $1/2$ between them for appropriate values of τ .

The quasi-momentum dependent topological Haldane mass, plays the most crucial role: it is the presence of a non-zero $M_H(\mathbf{k})$ that results in the appearance of areas of FZs in the complex z plane as well as the re-entrant behavior in the extreme slow limit. When $M_H(\mathbf{k})$ is switched off, the areas shrink to lines of FZs giving rise to an emergent one dimensional behavior with non-analyticities in $\text{Re}[f(t')]$ itself (and discontinuities in $\text{Re}[f'(t')]$) at those instants when these lines cut the real axis; furthermore, the re-entrant behavior completely disappears even in the extreme slow limit. Focussing on the re-entrant situation, if the value of $M_H(\mathbf{k})$ is slowly reduced, the areas corresponding to two branches of a lobe (for a given n) become thinner and thinner approaching two lines which eventually fall on top of each other when $M_H(\mathbf{k}) = 0$. We have also illustrated by considering hypothetical situations when the BZ is divided into regions with different (but constant within a region) M_H , how otherwise disjoint lines of Fisher zeros coalesce into dense areas in the real model with continuously varying M_H in the thermodynamic limit. Crucially, the critical rates τ_1^c and τ_2^c , marking the crossover between the no-DQPT, intermediate and re-entrant behavior of FZs are solely determined by the TRIM point included in the BZ for which $M_H = 0$, thereby, further emphasising the immense importance of the Haldane mass in dictating the nature of DQPTs.

A pertinent question that may arise at this point that how general the conclusion drawn based on the symmetry and topology will be, more because of the fact that numerical results are presented for a particular quenching protocol. Out of the three possible behaviour of DQPTs, what situation will be encountered depends upon the quenching amplitude for sudden quenching and the rate of quenching for the slow quenching case (between finite values of M_i and M_f). But what is robust is that there will be areas of FZs only when the Haldane mass has a continuous variation across the Brillouin zone for the present model. If it is altogether absent there will be lines of FZs. On the contrary, when it has a discrete variation over the BZ keeping the topological structure intact, there will be a deviation from the one-dimensional behaviour. These conclusions will hold true irrespective of the fact whether the quenching is sudden or slow or whether the DQPTs exist or not in the context of the model considered here.

Secondly, in the slow ramping case of the Haldane

model, the crossover rates τ_c^1 and τ_c^2 will always be determined by the excitation probabilities at the corner TRIM point ($k_x = k_y = 0$) and the central TRIM point of the BZ; the Haldane mass being zero at these points, the value of τ_c^1 and τ_c^2 are independent of the parameter ϕ for any-nonzero ϕ : to be precise, when $p_{\mathbf{k}}$ both at the corner TRIM point ($k_x = k_y = 0$) as well as at the central TRIM point exceed 0.5, there will be a no-DQPT behaviour while both these fall below 0.5, there will be an emergent (two-DQPTs) behaviour. Finally when $p_{\mathbf{k}} < 0.5$ at the corner point and exceeds 0.5 at the central point, there will be intermediate (one-DQPT) behaviour. In fact, the above argument would hold true for sudden quenches ($\tau = 0$) also; for example, one can conceive a sudden quenching scheme of the SM with $M_i = 2.6$ to $M_f = -2.6$; there will be an intermediate behaviour of FZs and hence one-DQPT. Analysing the corresponding analogue of Fig. (4c), one would find that the above arguments would explain the intermediate behaviour observed in this case. In summary, the observations concerning the importance of the Haldane mass and the importance of TRIM points in determining the occurrence of three different regions are robust and will be able to explain all the numerical findings in the context of the Haldane model.

Let us conclude with a few clarifying comments: (i) The graphene Hamiltonian with the SM (which has similarly been quenched) although anisotropic in k_x, k_y away from the DPs is still topologically trivial and does not lead to the generation of areas of FZs, essentially requiring the topological Haldane mass term to generate the areas. (ii) Furthermore, the addition of a hypothetical isotropic in k_x and k_y mass term such as $\cos(k_x^2 + k_y^2)$ alongwith the SM to the graphene Hamiltonian may generate areas of FZs in the complex z -plane. But such an isotropic mass term is non-topological. Since, our focus in this paper is strictly limited to the study of the topological Haldane model, where the quasi-momentum dependent Haldane mass term plays crucial role both in equilibrium topology and also in DQPTs, we do not consider such possibilities in this work. (iii) For slow quenching across a single critical point, when the M_H is present, the areas of FZs obviously show either no-DQPT or one-DQPT behaviour as has been shown in the sudden quenches case in [63] whereas when M_H is zero, here too FZs form lines. (iv) Finally, we would like to emphasize that in the infinite LZ limit ($M_i = -M_f \rightarrow \infty$), it can be argued that the effect of topology gets effectively wiped out.

Given the recent experimental observation of DQPTs as discussed in Sec. V, our work, naturally, opens up the possibility of further research in several new directions. One such example would be to explore the role of equilibrium topology in determining DQPTs in higher dimensional quenched topological models. Another intriguing question that inevitably needs to be addressed would be the effect of the edge states appearing in equilibrium topological models with open boundary condition,

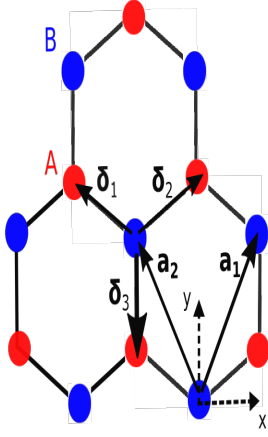


FIG. 9: A hexagonal lattice on which the topological Haldane model resides with \mathbf{a}_1 and \mathbf{a}_2 as the lattice vectors.

on the DQPTs described here.

Acknowledgements

We acknowledge interesting discussions with Shraddha Sharma. We also thankfully acknowledge G. Baskaran and A. Polkovnikov for critical comments. AD acknowledges financial support from SERB, DST, India.

Appendix A: A brief note on the Haldane model

We consider a 2D model on a hexagonal lattice comprised of two triangular sublattices A and B as shown in Figure 9. It can be understood as the composition of a nearest neighbour tight binding graphene-like Hamiltonian along with a Haldane mass (M_H) and sublattice symmetry (SLS) breaking Semenoff mass (M) term, with the Hamiltonian

$$\begin{aligned} \mathcal{H} = & t_1 \sum_{i,j=N1} \left(c_{iA}^\dagger c_{jB} + h.c. \right) \\ & + t_2 \sum_{i,j=N2} \left(e^{i\phi_{ij}} \left(c_{iA}^\dagger c_{jA} + c_{iB}^\dagger c_{jB} \right) + h.c. \right) \\ & + M \sum_{i \in A} \hat{n}_i - M \sum_{i \in B} \hat{n}_i. \end{aligned} \quad (\text{A1})$$

The $c_{iA(B)}$ s are spinless fermionic operators on sublattice A (B), and the t_2 s are the next nearest neighbour hopping interaction strengths. The time reversal symmetry of this model is broken by the phase factor $\phi_{ij} = \pm\phi$, originating from the staggered magnetic field and is positive for anticlockwise next nearest neighbour hopping.

Fourier transforming into \mathbf{k} -space the Hamiltonian becomes

$$\mathcal{H} = \begin{pmatrix} c_A^\dagger(\mathbf{k}) & c_B^\dagger(\mathbf{k}) \end{pmatrix} \mathbf{h}(\mathbf{k}) \begin{pmatrix} c_A(\mathbf{k}) \\ c_B(\mathbf{k}) \end{pmatrix}, \quad (\text{A2})$$

where

$$\mathbf{h}(\mathbf{k}) = \sum_{i=0}^3 h_i(\mathbf{k}) \sigma_i. \quad (\text{A3})$$

The σ_i , $i \in \{1, 2, 3\}$ are the Pauli matrices, σ_0 is the identity matrix and a is the lattice constant. We have

$$\begin{aligned} h_0 = & 2t_2 \cos(\phi) \left[\cos(\mathbf{k} \cdot \mathbf{a}_1) + \cos(\mathbf{k} \cdot \mathbf{a}_2) \right. \\ & \left. + \cos(\mathbf{k} \cdot (\mathbf{a}_1 - \mathbf{a}_2)) \right], \end{aligned} \quad (\text{A4})$$

$$\begin{aligned} h_1 = & t_1 \left[1 + \cos(\mathbf{k} \cdot \mathbf{a}_1) + \cos(\mathbf{k} \cdot \mathbf{a}_2) \right] \\ h_2 = & t_1 \left[\sin(\mathbf{k} \cdot \mathbf{a}_1) + \sin(\mathbf{k} \cdot \mathbf{a}_2) \right], \end{aligned} \quad (\text{A5})$$

$$h_3 = M + M_H, \quad (\text{A6})$$

$$\begin{aligned} M_H = & 2t_2 \sin(\phi) \left[\sin(\mathbf{k} \cdot \mathbf{a}_2) - \sin(\mathbf{k} \cdot \mathbf{a}_1) \right. \\ & \left. + \sin(\mathbf{k} \cdot (\mathbf{a}_1 - \mathbf{a}_2)) \right], \end{aligned} \quad (\text{A7})$$

where $\mathbf{a}_1 = \frac{a}{2} (3, \sqrt{3})$ and $\mathbf{a}_2 = \frac{a}{2} (-3, \sqrt{3})$ as shown in Figure 9.

- [1] I. Bloch, J. Dalibard, and W. Zwerger, Rev. Mod. Phys. **80**, 885 (2008).
- [2] M. Lewenstein, A. Sanpera, and V. Ahufinger, (Oxford University Press, Oxford (2012)).
- [3] M. Greiner, O. Mandel, T. W. Hansch and I. Bloch, Nature **419**, 51 (2002).
- [4] T. Kinoshita, T. Wenger and D. S. Weiss, Nature **440**,

- 900 (2006).
- [5] M. Gring, M. Kuhnert, T. Langen, T. Kitagawa, B. Rauer, M. Schreitl, I. Mazets, D. Adu Smith, E. Demler, and J. Schmiedmayer, Science **337**, 1318 (2012).
- [6] S. Trotzky, Y-A. Chen, A. Flesch, I. P. McCulloch, U. Schollwck, J. Eisert and I. Bloch, Nature **8**, 325 (2012).
- [7] M. Cheneau, P. Barmettler, D. Poletti, M. Endres, P.

- Schauss, T. Fukuhara, C. Gross, I. Bloch, C. Kollath and S. Kuhr, *Nature* **481**, 484 (2012).
- [8] D. Fausti, R. I. Tobey, N. Dean, S. Kaiser, A. Dienst, M. C. Hoffmann, S. Pyon, T. Takayama, H. Takagi, A. Cavalleri, *Science* **331**, 189 (2011).
- [9] M. C. Rechtsman, J. M. Zeuner, Y. Plotnik, Y. Lumer, D. Podolsky, F. Dreisow, S. Nolte, M. Segev and A. Szameit, *Nature* **496** 196 (2013).
- [10] M. Schreiber, S. S. Hodgman, P. Bordia, Henrik P. Lschen, M. H. Fischer, R. Vosk, E. Altman, U. Schneider, I. Bloch, *Science* **349**, 842 (2015).
- [11] P. Calabrese, and J. Cardy, *Phys. Rev. Lett.* **96**, 136801 (2006); *J. Stat. Mech.* P06008 (2007).
- [12] M. Rigol, V. Dunjko and M. Olshanii, *Nature* **452**, 854 (2008).
- [13] T Oka, H Aoki, *Phys. Rev. B* **79** 081406 (2009).
- [14] T. Kitagawa, E. Berg, M. Rudner, and E. Demler, *Phys. Rev. B* **82**, 235114 (2010).
- [15] N. H. Lindner, G. Refael and V. Galitski, *Nat. Phys.* **7**, 490-495, (2011).
- [16] A. Bermudez, D. Patane, L. Amico, M. A. Martin-Delgado, *Phys. Rev. Lett.* **102**, 135702, (2009).
- [17] A. A. Patel, S. Sharma, A. Dutta, *Eur. Phys. Jour. B* **86**, 367 (2013); A. Rajak and A. Dutta, *Phys. Rev. E* **89**, 042125, 2014. P. D. Sacramento, *Phys. Rev. E* **90** 032138, (2014); M. D. Caio, N. R. Cooper and M. J. Bhaseen, *Phys. Rev. Lett.* **115**, 236403 (2015).
- [18] M. Thakurathi, A. A. Patel, D. Sen, and A. Dutta, *Phys. Rev. B* **88**, 155133 (2013).
- [19] V. Mukherjee and A. Dutta, *J. Stat. Mech.* P05005 (2009).
- [20] A. Das, *Phys. Rev. B* **82**, 172402 (2010).
- [21] A. Russomanno, A. Silva and G. E. Santoro, *Phys. Rev. Lett.* **109**, 257201 (2012); S. Sharma, A. Russomanno, G. E. Santoro and A. Dutta, *EPL* **106**, 67003 (2014).
- [22] A. Sen, S. Nandy, K. Sengupta, *Phys. Rev. B* **94**, 214301 (2016).
- [23] M. Bukov, L. D'Alessio and A. Polkovnikov, *Adv. Phys.* **64**, No. 2, 139-226 (2016).
- [24] A Pal and DA Huse, *Phys. Rev. B* **82**, 174411 (2010).
- [25] R. Nandkishore, D. A. Huse, *Annual Review of Condensed Matter Physics*, **6**, 15-38 (2015).
- [26] J. Dziarmaga, *Advances in Physics* **59**, 1063 (2010).
- [27] A. Polkovnikov, K. Sengupta, A. Silva, and M. Vengalattore, *Rev. Mod. Phys.* **83**, 863 (2011).
- [28] A. Dutta, G. Aeppli, B. K. Chakrabarti, U. Divakaran, T. Rosenbaum and D. Sen, *Quantum Phase Transitions in Transverse Field Spin Models: From Statistical Physics to Quantum Information* (Cambridge University Press, Cambridge, 2015).
- [29] J. Eisert, M. Friesdorf and C. Gogolin, *Nat. Phys.* **11**, 124 (2015).
- [30] L. D'Alessio, Y. Kafri, A. Polkovnikov, M. Rigol, *Adv. Phys.* **65**, 239 (2016).
- [31] *J. Stat. Mech.: Theo. and Expt*, special issue *Quantum Integrability in Out of Equilibrium Systems* edited by P. Calabrese., F. H. L. Essler and G. Mussardo, **2016** (2016).
- [32] M. Heyl, A. Polkovnikov, and S. Kehrein, *Phys. Rev. Lett.*, **110**, 135704 (2013).
- [33] S. Sachdev, (Cambridge University Press, Cambridge, UK, 2010).
- [34] M.E. Fisher, in *Boulder Lectures in Theoretical Physics* (University of Colorado, Boulder, 1965), Vol. 7.
- [35] C. Yang and T. Lee, *Phys. Rev.* **87**, 404 (1952).
- [36] W. van Saarloos and D. Kurtze, *J. Phys. A* **17**, 1301 (1984).
- [37] S. Suzuki, J-i Inoue and Bikas K. Chkarabarti, (Springer, Lecture Notes in Physics, Vol. 862 (2013)).
- [38] C. Karrasch and D. Schuricht, *Phys. Rev. B*, **87**, 195104 (2013).
- [39] N. Kriel, C. Karrasch, and S. Kehrein, *Phys. Rev. B* **90**, 125106 (2014).
- [40] M. Heyl, *Phys. Rev. Lett.*, **113**, 205701 (2014).
- [41] F. Andraschko, J. Sirker, *Phys. Rev. B* **89**, 125120 (2014).
- [42] E. Canovi, P. Werner, and M. Eckstein, *Phys. Rev. Lett.* **113**, 265702 (2014).
- [43] M. Heyl, *Phys. Rev. Lett.*, **115**, 140602 (2015).
- [44] T. Palmai, *Phys. Rev. B* **92**, 235433 (2015).
- [45] U. Divakaran, S. Sharma and A. Dutta, *Phys. Rev. E* **93**, 052133 (2016).
- [46] Z. Huang, and A. V. Balatsky, *Phys. Rev. Lett.* **117**, 086802 (2016).
- [47] T. Puskarov and D. Schuricht, arXiv: 1608.05584 (2016).
- [48] J. M. Zhang abd H.-T. Yang, arXiv: 1605.05403 (2016).
- [49] M. Heyl, *Phys. Rev. B* **95**, 060504 (2017).
- [50] Bojan Zunkovic, Markus Heyl, Michael Knap, Alessandro Silva, arXiv:1609.08482 (2016).
- [51] A.A. Zvyagin, arXiv:1701.08851 (2017).
- [52] T. Obuchi, S. Suzuki, K. Takahashi, arXiv:1702.05396 (2017).
- [53] Thoms Fogarty, Ayaka Usui, Thomas Busch, Alessandro Silva, John Gool, arXiv:1704.07659 (2017).
- [54] S. Vajna and B. Dora, *Phys. Rev. B* **89**, 161105(R) (2014).
- [55] S. Sharma, S. Suzuki and A. Dutta, *Phys. Rev. B* **92**, 104306 (2015).
- [56] J. C. Budich and M. Heyl, *Phys. Rev. B* **93**, 085416 (2016).
- [57] F. Pollmann, S. Mukerjee, A. G. Green, and J. E. Moore, *Phys. Rev. E* **81**, 020101(R) (2010).
- [58] S. Sharma, U. Divakaran, A. Polkovnikov and A. Dutta, *Phys. Rev. B* **93**, 144306 (2016).
- [59] T. W. B. Kibble, *J. Phys. A* **9**, 1387 (1976).
- [60] W. H. Zurek, *Nature* **317**, 505 (1985).
- [61] W. H. Zurek, U. Dorner, and P. Zoller, *Phys. Rev. Lett.* **95**, 105701 (2005).
- [62] A. Polkovnikov, *Phys. Rev. B* **72**, 161201(R) (2005).
- [63] S. Vajna and B. Dora, *Phys. Rev. B* **91**, 155127 (2015).
- [64] M. Schmitt and S. Kehrein, *Phys. Rev. B* **92**, 075114 (2015).
- [65] H.T. Quan, Z. Song, X.F. Liu, P. Zanardi, and C.P. Sun, *Phys. Rev. Lett.* **96**, 140604 (2006).
- [66] D. Rossini, T. Calarco, V. Giovannetti, S. Montangero, R. Fazio, *Phys. Rev. A* **75**, 032333 (2007).
- [67] F. M. Cucchietti, *et al*, *Phys. Rev. A* **75**, 032337 (2007); C. Cormick and J. P. Paz, *Phys. Rev. A* **77**, 022317 (2008).
- [68] S. Sharma, V. Mukherjee, and A. Dutta, *Eur. Phys. J. B*, **85**, 143 (2012).
- [69] Lorenzo C Venuti and P. Zanardi, *Phys. Rev. A* **81**, 022113 (2010); Lorenzo C. Venuti, N. T. Jacobson, S. Santra, and P. Zanardi, *Phys. Rev. Lett.* **107**, 010403 (2011).
- [70] V. Mukherjee, S. Sharma, A. Dutta, *Phys. Rev. B* **86**, 020301 (R) (2012).
- [71] T. Nag, U. Divakaran and A. Dutta, *Phys. Rev. B* **86**,

- 020401 (R) (2012); S. Suzuki, T. Nag and A. Dutta, Phys. Rev. A **93**, 012112(2016)
- [72] B. Dora, F. Pollmann, J. Fortgh, G. Zarand, Phys. Rev. Lett. **111**, 046402 (2013); R. Sachdeva, T. Nag, A. Agarwal, A. Dutta, Phys. Rev. B **90**, 045421 (2014).
- [73] A. Gambassi and A. Silva, arXiv: 1106.2671 (2011); , Phys. Rev. Lett. **109**, 250602 (2012); P. Smacchia and A. Silva, Phys. Rev. E **88**, 042109, (2013).
- [74] A. Russomanno, S. Sharma, A. Dutta and G. E. Santoro, J. Stat. Mech., P08030 (2015).
- [75] P. Zanardi, H. T. Quan, X. Wang and C. P. Sun, Phys. Rev. A **75**, 032109 (2007).
- [76] R. Dorner, J. Goold, C. Cormick, M. Paternostro and V. Vedral, Phys. Rev. Lett. **109**, 160601 (2012).
- [77] S. Sharma and A. Dutta, Phys. Rev. E **92**, 022108 (2015).
- [78] N. Flaschner, D. Vogel, M. Tarnowski, B. S. Rem, D.-S. Luhmann, M. Heyl, J. Budich, L. Mathey, K. Sengstock, C. Weitenberg, arXiv:1608.05616 (2016).
- [79] P. Jurcevic, H. Shen, P. Hauke, C. Maier, T. Brydges, C. Hempel, B. P. Lanyon, M. Heyl, R. Blatt, C. F. Roos, arXiv:1612.06902 (2016).
- [80] M. Haldane, Phys. Rev. Lett. **61**, 2015, (1988).
- [81] G. Jotzu , M. Messer, R. Desbuquois, M. Lebrat, T. Uehlinger, D. Greif and T. Esslinger, Nature **515**, 237 (2014).
- [82] M. Aidelsburger, M. Lohse, C. Schweizer, M. Atala, J. T. Barreiro, S. Nascimbene, N. R. Cooper, I. Bloch and N. Goldman, Nature Physics **11**, 162 (2015).
- [83] G. Semenoff, Phys. Rev. Lett. **53**, 2449 (1984). G. W. Semenoff, V. Semenoff, and Fei Zhou, Phys. Rev. Lett. **101**, 087204 (2008).
- [84] L. Privitera and G. E. Santoro, Phys. Rev. B **93**, 241406(R)(2016).
- [85] C. Zener, Proc. Roy. Soc. London Ser A **137**, 696 (1932); L. D. Landau and E. M. Lifshitz, *Quantum Mechanics: Non-relativistic Theory*, 2nd ed. (Pergamon Press, Oxford, 1965).
- [86] S. Suzuki and M. Okada, in *Quantum Annealing and Related Optimization Methods*, Ed. by A. Das and B. K. Chakrabarti (Springer-Verlag, Berlin, 2005), p. 185.
- [87] N. V. Vitanov and B. M. Garraway, Phys. Rev. A **53**, 4288 (1996); N. V. Vitanov, *ibid.* **59**, 988 (1999).
- [88] X. Peng, H. Zhou, B.-B. Wei, J. Cui, J. Du, and R.-B. Liu, Phys. Rev. Lett. **114**, 010601 (2015).